

Temperature and current sensitivity extraction of optical superconducting transition-edge sensorsbased on a two-fluid model

Yue Geng(耿悦), Pei-Zhan Li(李佩展), Jia-Qiang Zhong(钟家强), Wen Zhang(张文), Zheng Wang(王争), Wei Miao(缪巍), Yuan Ren(任远), and Sheng-Cai Shi(史生才)

Citation: Chin. Phys. B, 2021, 30 (**9**): 098501. DOI: 10.1088/1674-1056/ac11ce
Journal homepage: http://cpb.iphy.ac.cn; http://iopscience.iop.org/cpb

What follows is a list of articles you may be interested in

Wavelength dependence of intrinsic detection efficiency of NbN superconducting nanowire single-photon detector

Yong Wang(王勇), Hao Li(李浩), Li-Xing You(尤立星), Chao-Lin Lv(吕超林), He-Qing Wang(王河清), Xing-Yu Zhang(张兴雨), Wei-Jun Zhang(张伟君), Hui Zhou(周慧), Lu Zhang(张露), Xiao-Yan Yang(杨晓燕), Zhen Wang(王镇)

Chin. Phys. B, 2019, 28 (**7**): 078502. DOI: 10.1088/1674-1056/28/7/078502

Photon-counting chirped amplitude modulation lidar system using superconducting nanowire single-photon detector at 1550-nm wavelength

Hui Zhou(周慧), Yu-Hao He(何宇昊), Chao-Lin Lü(吕超林), Li-Xing You(尤立星), Zhao-Hui Li(李召辉), Guang Wu(吴光), Wei-Jun Zhang(张伟君), Lu Zhang(张露), Xiao-Yu Liu(刘晓宇), Xiao-Yan Yang(杨晓燕), Zhen Wang(王镇)

Chin. Phys. B, 2018, 27 (**1**): 018501. DOI: 10.1088/1674-1056/27/1/018501

Bias-dependent timing jitter of 1-GHz sinusoidally gated InGaAs/InP avalanche photodiode

Ge Zhu(朱阁), Fu Zheng(郑福), Chao Wang(王超), Zhibin Sun(孙志斌), Guangjie Zhai(翟光杰), Qing Zhao(赵清)

Chin. Phys. B, 2016, 25 (**11**): 118505. DOI: 10.1088/1674-1056/25/11/118505

High efficiency, large-active-area superconducting nanowire single-photon detectors

Gu Min, Zhang La-Bao, Kang Lin, Zhao Qing-Yuan, Jia Tao, Wan Chao, Xu Rui-Ying, Yang Xiao-Zhong, Wu Pei-Heng, Zhang Yong, Xia Jin-Song

Chin. Phys. B, 2015, 24 (**6**): 068501. DOI: 10.1088/1674-1056/24/6/068501

Optical response of Al/Ti bilayer transition edge sensors

Zhang Qing-Ya, Wang Tian-Shun, Liu Jian-She, Dong Wen-Hui, He Gen-Fang, Li Tie-Fu, Zhou Xing-Xiang, Chen Wei

Chin. Phys. B, 2014, 23 (**11**): 118502. DOI: 10.1088/1674-1056/23/11/118502

Temperature and current sensitivity extraction of optical superconducting transition-edge sensors based on a two-fluid model*

Yue Geng(耿悦)[1,2,3], Pei-Zhan Li(李佩展)[1,2,3], Jia-Qiang Zhong(钟家强)[1,3], Wen Zhang(张文)[1,3,†], Zheng Wang(王争)[1,3], Wei Miao(缪巍)[1,3], Yuan Ren(任远)[1,3], and Sheng-Cai Shi(史生才)[1,3,‡]

[1] *Purple Mountain Observatory, Chinese Academy of Sciences, Nanjing* 210023, *China*
[2] *University of Science and Technology of China, Hefei* 230026, *China*
[3] *Key Laboratory of Radio Astronomy, Chinese Academy of Sciences, Nanjing* 210023, *China*

(Received 30 March 2021; revised manuscript received 23 June 2021; accepted manuscript online 7 July 2021)

Optical superconducting transition-edge sensor (TES) has been widely used in quantum information, biological imaging, and fluorescence microscopy owing to its high quantum efficiency, low dark count, and photon number resolving capability. The temperature sensitivity (α_I) and current sensitivity (β_I) are important parameters for optical TESs, which are generally extracted from the complex impedance. Here we present a method to extract α_I and β_I based on a two-fluid model and compare the calculated current–voltage curves, pulse response, and theoretical energy resolution with the measured ones. This method shows qualitative agreement that is suitable for further optimization of optical TESs.

Keywords: transition-edge sensor, single-photon detector, two-fluid model

PACS: 85.25.Oj, 85.25.Am **DOI:** 10.1088/1674-1056/ac11ce

1. Introduction

Superconducting transition-edge sensors (TESs) are capable to resolve the energy of a single optical/near-infrared (NIR) photon and have been used in quantum information,[1] biological imaging,[2] and fluorescence microscopy.[3] Optical TESs have exhibited a system quantum efficiency of nearly 100% at optical/NIR wavelengths.[4,5] Titanium (Ti) TES with a critical temperature (T_C) of 470 mK shows a time constant as short as 0.2 μs,[6] making MHz counting rate possible in photon metrology fields, while high-energy resolution (ΔE) is necessary for quantum-key distribution applications. To improve ΔE, one can develop optical TESs with small heat capacity (C) or low T_C. For a 25-μm square tungsten TES with a T_C of 178 mK, a ΔE of 0.29 eV has been achieved,[4] while a 10-μm square Ti/Au bilayer TES with a T_C of 105 mK exhibits a ΔE of 0.113 eV.[7] The theoretical ΔE can be written as[8]

$$\Delta E = 2\sqrt{2\ln 2}\sqrt{4k_B T_0^2 \frac{C}{\alpha_I}\sqrt{n(1+2\beta_I)/2}}, \tag{1}$$

where k_B is the Boltzmann constant; n is the material-dependent exponent for the thermal conductivity; T_0 is the electron temperature; $\alpha_I = \frac{T_0}{R_0}\frac{dR}{dT}\Big|_{I_0}$ is the temperature sensitivity, and $\beta_I = \frac{I_0}{R_0}\frac{dR}{dI}\Big|_{T_0}$ is the current sensitivity. The working point of a TES is described by current (I_0), voltage (V_0), resistance ($R_0 = V_0/I_0$), and temperature (T_0). To calculate ΔE theoretically using Eq. (1), one needs to know all the parameters. Some of these parameters, such as V_0, I_0, R_0, T_C, normal-state resistance (R_n), thermal conductance (G), and n, can be extracted from the current–voltage (I–V) curves measured at different bath temperatures (T_{bath}), while C, α_I, and β_I are generally obtained from complex impedance measurement.[9] However, it is quite difficult to perform such experiments because optical TESs response very fast, and the complex impedance has to be measured up to a few tens of MHz, where parasitic effects (including capacitance and inductance) and reflections due to the discontinuities in the characteristic impedance of transmission lines in the readout electronics become significant.[10] Here we present an alternative method to extract α_I and β_I based on a two-fluid model and compare the calculated I–V curves, pulse response, and theoretical ΔE with the measured ones.

2. Extraction of parameters

Firstly, we introduce the two-fluid model that separates the sensor's current into a superconducting component and a quasiparticle component, from which α_I and β_I can be calculated, and then C is extracted in combination with the measured pulse response.

*Project supported by the National Key Basic Research and Development Program of China (Grant No. 2017YFA0304003), the National Natural Science Foundation of China (Grant Nos. U1831202, U1731119, U1931123, 11773083, and 11873099), the Chinese Academy of Sciences (Grant Nos. QYZDJ-SSW-SLH043 and GJJSTD20180003), and Jiangsu Province, China (Grant No. BRA2020411).

†Corresponding author. E-mail: wzhang@pmo.ac.cn
‡Corresponding author. E-mail: scshi@pmo.ac.cn

© 2021 Chinese Physical Society and IOP Publishing Ltd

2.1. Two-fluid model

In the two-fluid model, the total current through a TES is described as a combination of a normal and a supercurrent, $I_0 = C_I I_C + V_0/(C_R R_n)$,[11] where C_I is the supercurrent to critical current (I_C) ratio and $C_R = 2N\rho\Lambda_Q/R_n$, in which ρ is the normal-state resistance per unit length, Λ_Q is the charge imbalance relaxation length, and N is the number of phase-slip lines. The TES resistance can be expressed as[12]

$$R(V_0, T_0) = \left(\frac{C_I I_{C0} \left(1 - (T_0/T_C)\right)^{3/2}}{V_0} + \frac{1}{C_R R_n} \right)^{-1}, \quad (2)$$

where I_{C0} is the zero-temperature I_C of the film.[11] The two-fluid model relates α_I and β_I to the two key parameters

$$\alpha_I = \frac{3}{2} \frac{C_R R_n}{R_0} \frac{C_I I_{C0}}{I_0} \frac{T_0}{T_C} \left(1 - \frac{T_0}{T_C}\right)^{1/2}, \quad (3)$$

$$\beta_I = C_R \frac{R_n}{R_0} - 1. \quad (4)$$

The results of this model agree well with experimental results[13,14] by treating C_I and C_R as constants across the transition. Here we treat them as variables and fit the data points on the I–V curves to Eq. (2) to obtain these parameters as a function of reduced resistance (R_0/R_n) based on the two-fluid model. Subsequently α_I and β_I can be calculated using Eqs. (3) and (4) from C_I and C_R obtained above.

2.2. Optical TESs and measurement setup

The optical TESs were made of a 30.3-nm-thick Ti film deposited using electron-beam evaporation in high vacuum,[15] and active areas between 5×5 μm^2 and 20×20 μm^2 are patterned by optical lithography using lift-off process. An optical cavity consisting of a dielectric mirror (DM) and antireflection (AR) coatings is integrated with the TESs to improve the absorption efficiency.[16] The TES device is mounted in a dilution refrigerator at a base temperature of 20 mK, and a 110 mΩ shunt resistor in parallel with the TES is used to realize the constant voltage bias. The TES current is read out by a superconducting quantum interference device (SQUID) current amplifier with a flux-locked loop. We have tested several Ti TESs with different active areas, R_n and T_C, and obtained similar results. Therefore we just compare the calculated parameters with the measured ones for a 20-μm square Ti TES device below.

2.3. $C_I I_{C0}$ and C_R

Figure 1 shows the measured I–V curves at different T_{bath} between 100 mK and 210 mK. By fitting the measured data points at a constant R_0 to the power flow equation $P_{DC} = I_0 V_0 = K(T_0^n - T_{bath}^n)$, some useful parameters (such as K, n and T_C) are obtained, and then G is derived from $G = nKT_0^{n-1}$. These parameters are listed in Table 1.

Table 1. Parameters of the 20-μm^2 Ti TES at $R_0 = 0.48R_n$ and 100 mK.

n	G (pW/K)	I_{C0} (mA)	C_I	C_R	α_I	β_I	$\wp$	τ_{el} (μs)	τ_{eff} (μs)	C (fJ/K)
5.2	110	1.9	0.81	0.56	96	0.16	18	0.15	2.8	4.7

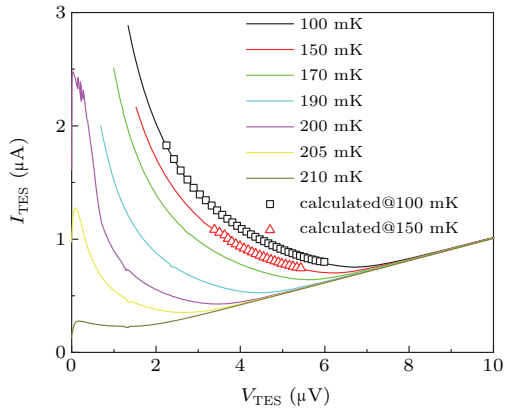


Fig. 1. Measured and calculated current–voltage curves of the Ti TES at different bath temperatures.

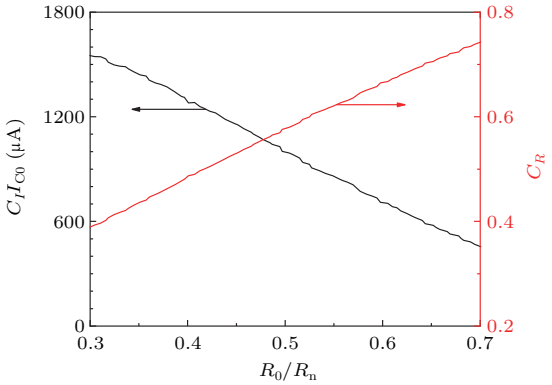


Fig. 2. Extracted $C_I I_{C0}$ and C_R of the optical TES as a function of R_0/R_n at 100 mK.

Suppose that $C_I I_{C0}$ and C_R change with working points (I_0, V_0, R_0), then we can fit the data points on the I–V curve at a bath temperature of 100 mK to obtain $C_I I_{C0}$ and C_R. As shown in Fig. 2, $C_I I_{C0}$ decreases with the resistance while C_R increases as expected.

2.4. α_I and β_I

Since $C_I I_{C0}$ and C_R are known, α_I and β_I can be calculated using Eqs. (3) and (4). As shown in Fig. 3 the resistance

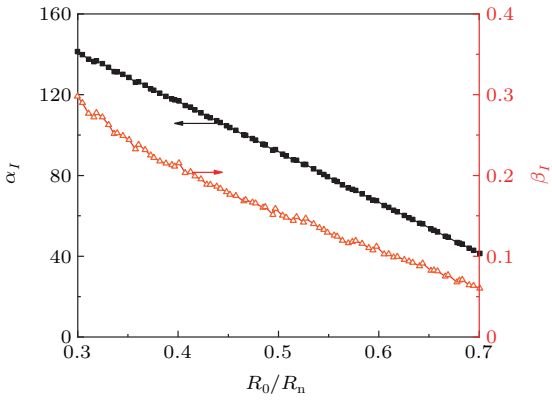


Fig. 3. Calculated α_I and β_I as a function of R_0/R_n for the Ti TES at 100 mK.

dependence of α_I and β_I is similar to that predicted by complex impedance measurements in other experiments.[10,17]

2.5. Thermal capacity

The response of the Ti TES to 1550-nm photons irradiated by an ultra-short pulsed laser source is measured. The output response curves are recorded by a digital oscilloscope (see Fig. 4(a)). By fitting the response curve to a double-exponential function,[18] electrical time constant ($\tau_{\rm el}$) and effective thermal time constant ($\tau_{\rm eff}$) are determined to be 0.15 μs and 2.8 μs, respectively. $\tau_{\rm eff}$ is theoretically described as[8]

$$\tau_{\rm eff} = \frac{C}{G}\frac{1+\beta_I+R_{\rm bias}/R_0}{1+\beta_I+R_{\rm bias}/R_0+(1-R_{\rm bias}/R_0)\wp}, \tag{5}$$

where $\wp = \left(I_0^2 R_0 \alpha_I\right)/(GT_0)$ is the loop gain. Figure 4(b) plots the heat capacity C extracted from the obtained $\tau_{\rm eff}$, α_I, and β_I. As can be seen from Fig. 4(b), C at high bias points ($\sim 0.7R_{\rm n}$) is smaller than that at low bias points ($\sim 0.3R_{\rm n}$) close to the superconducting state. The theoretical C of the TES device is estimated to be ~ 2 fJ/K by taking a factor of 2.43 into account. The obtained C is larger than the theoretical one, which is possibly attributed to the property deviation of thin-film from bulk ones. In addition, impurities introduced in the fabrication of TES device can also increase C, which has been confirmed by complex impedance measurement.[9,19]

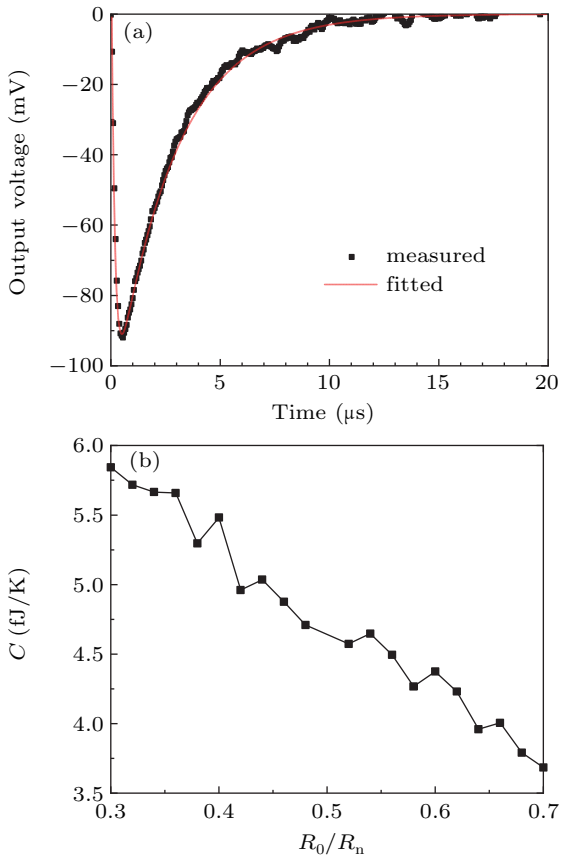


Fig. 4. (a) Measured pulse response of the Ti TES at 0.48 $R_{\rm n}$ and 100 mK. (b) Obtained heat capacity as a function of $R_0/R_{\rm n}$ for the Ti TES at 100 mK.

With the obtained C, the critical current of the TES device is calculated to be $I_{\rm C0} = 3.52\sqrt{\frac{k_{\rm B}C}{\hbar R_{\rm n}}}T_{\rm C} = 1.9$ mA.[11] As a result, C_I is separated from the product of $C_I I_{\rm C0}$. C_I is 0.81 at $0.3R_{\rm n}$ and decreases linearly to 0.24 at $0.7R_{\rm n}$. The important parameters of the TES device at $0.48R_{\rm n}$ and 100 mK have been provided in Table 1.

3. Discussion

With the extracted parameters, we calculate the I–V curves, α, pulse response height, and ΔE, and compare them to the measurement results. As shown in Fig. 1, the calculated I–V curves of the TES at 100 mK and 150 mK fit well with the measured data points. The total sensitivity $\alpha_{\rm total}$, obtained through the derivative of the measured I–V curve (i.e., $({\rm d}V/{\rm d}I - R_0)/({\rm d}V/{\rm d}I + R_0)$), is a function of α_I and β_I[10]

$$\alpha_{\rm total} = \frac{2\alpha_I + \frac{GT_0}{I_0^2 R_0}\beta_I}{2+\beta_I}. \tag{6}$$

Figure 5 shows $\alpha_{\rm total}$ from the measured I–V curve as well as from the extracted α_I and β_I, which is clearly in good agreement except for a little discrepancy when biasing at lower R.

Another consistency check has been done with respect to the pulse response height. The pulse response can be expressed as[8]

$$U(t) = A\left(\frac{\tau_I}{\tau_{\rm el}}-1\right)\left(\frac{\tau_I}{\tau_{\rm eff}}-1\right) \times \frac{1}{2+\beta_I}\frac{C\delta T}{I_0 R_0 \tau_I^2}\frac{{\rm e}^{-t/\tau_{\rm el}} - {\rm e}^{-t/\tau_{\rm eff}}}{1/\tau_{\rm el} - 1/\tau_{\rm eff}}, \tag{7}$$

where A is the gain of readout electronics and $\tau_I = \tau/(1-\wp)$ is the current-biased thermal time constant with the intrinsic time constant ($\tau = C/G$). We calculate the pulse response height in response to a 1550-nm photon ($E_\gamma = C\delta T = 0.8$ eV), and plot the calculated height as a function of $R_0/R_{\rm n}$ in Fig. 6, where the measured height is also plotted for comparison. The difference between them comes from the energy collection efficiency.

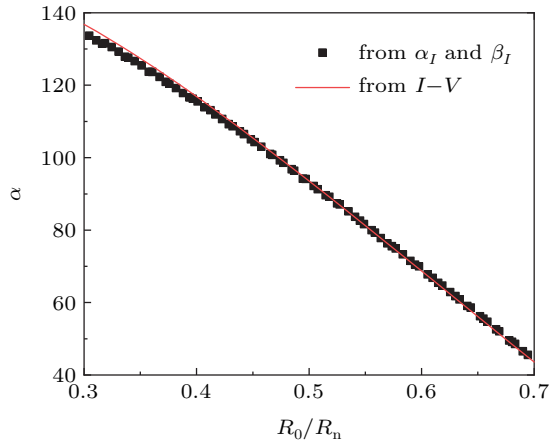


Fig. 5. Total sensitivity $\alpha_{\rm total}$ from the two-fluid model and calculated from I–V of the TES at 100 mK.

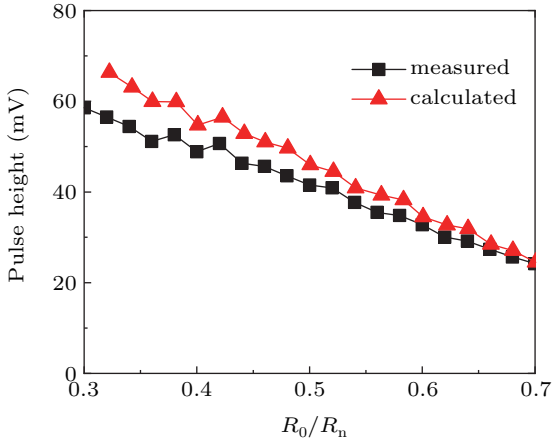


Fig. 6. Measured and calculated pulse height of the TES at 100 mK.

Figure 7(a) illustrates the pulse height distribution of the optical TES in response to the 1550-nm pulsed laser source, attenuated to an average of $\mu_{in} = 1.79$ photons per pulse. Our optical TES can discriminate each photon state, up to 4 photons per pulse. The coherent laser source has a possibility of producing an n-photon state given by Poisson distribution, while the detected signal satisfies a Gaussian distribution. Therefore, the pulse height distribution can be modeled as a convolution of Poisson distribution with Gaussian distribution[21]

$$y = \frac{B\mathrm{e}^{-\mu}}{\sqrt{2\pi\sigma_E^2}}\left[\frac{\sigma_E}{\sigma_0}\exp\left(-\frac{(x-x_0)^2}{2\sigma_0^2}\right) + \sum_{i=1}^{n}\frac{\mu^i}{i!}\exp\left(-\frac{(x-x_i)^2}{2\sigma_E^2}\right)\right], \tag{8}$$

where B is a normalization factor, μ is the average number of detected photons per pulse of the incident light, and i is the number of absorbed photons that generate the signal centered on amplitude equal to x_i. The same variance (σ_E) for each peak is assumed except for the first one in which we use an appropriate spread (σ_0), corresponding to the case of no-photons detected. ΔE is related to σ_E by

$$\Delta E = 2.355\frac{\sigma_E}{x_2 - x_1}E_\gamma. \tag{9}$$

By fitting the measured data to Eq. (8), we obtain $\mu = 1.09$. Therefore, the system quantum efficiency is $\eta_{sys} = \mu/\mu_{in} = 61\%$. The measured ΔE is 0.52 eV using Eq. (9). We subsequently measure ΔE at other working points. As shown in Fig. 7(b), ΔE is relatively flat at a working point below $0.5R_n$, and above $0.5R_n\Delta E$ increases. Theoretical energy resolution (ΔE_{th}) is calculated according to Eq. (1) given the parameters obtained from the two-fluid model. As shown in Fig. 7(b), ΔE_{th} is about 0.27 eV at low resistance. There is a significant difference between theoretical and measured ΔE. The current noise of ~ 20 pA/Hz$^{0.5}$ measured in the TES at R_n is much higher than the SQUID's nominal current noise of ~ 5 pA/Hz$^{0.5}$, which indicates that some excess noise comes from our refrigerator and electronics.[22] As a result, it gives rise to a higher measured value of ΔE than the theoretical one. To further improve ΔE, it is necessary to decrease its C (i.e., the volume of the active area) or T_C by baking the TES.[22]

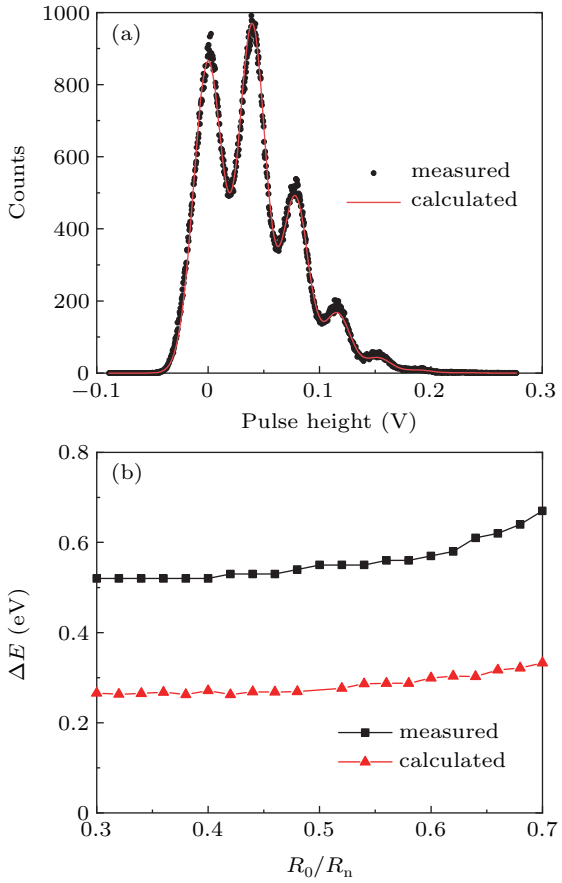


Fig. 7. (a) Pulse height histogram. (b) Measured and calculated ΔE.

4. Conclusion

In this paper, we extracted the key parameters of optical TESs based on the two-fluid model by treating C_I and C_R as variables in the transition, which gives a similar accuracy to complex impedance measurement. With this method, the calculated I–V curves and pulse responses are consistent with the measured ones. The theoretical ΔE of 0.27 eV is about 52% of the measured one, which can be attributed to the excess readout noise. In order to further improve ΔE, we will fabricate optical TESs with smaller active area or depress T_C by baking it in air.

Acknowledgment

The authors would like to thank Jin-Feng Wang of Nanjing Institute of Astronomical Optics and Technology and Wei-Dong Shen of Zhejiang University for fabricating the optical cavity of TESs.

References

[1] Giustina M, Versteegh M A M, Wengerowsky S, Handsteiner J, Hochrainer A, Phelan K, Steinlechner F, Kofler J, Larsson J, Abellán C, Amaya W, Pruneri V, Mitchell M W, Beyer J, Gerrits T, Lita A E, Shalm L K, Nam S W, Scheidl T, Ursin R, Wittmann B and Zeilinger A 2015 *Phys. Rev. Lett.* **115** 250401

[2] Niwa K, Numata T, Hattori K and Fukuda D 2017 *Sci. Rep.* **7** 45660

[3] Fukuda D, Niwa K, Hattori K, Inoue S, Kobayashi R and Numata T 2018 *J. Low Temp. Phys.* **193** 1228

[4] Lita A E, Miller A J and Nam S W 2008 *Opt. Express* **16** 3032

[5] Fukuda D, Fujii G, Numata T, Amemiya K, Yoshizawa A, Tsuchida H, Fujino H, Ishii H, Itatani T, Inoue S and Zama T 2011 *Opt. Express* **19** 870

[6] Portesi C, Taralli E, Lolli L, Rajteri M and Monticone E 2015 *IEEE Trans. Appl. Supercond.* **25** 1

[7] Lolli L, Taralli E, Portesi C, Monticone E and Rajteri M 2013 *Appl. Phys. Lett.* **103** 041107

[8] Irwin K D and Hilton G C 2005 *Transition-Edge Sensors in Cryogenic Particle Detection* (Berlin: Springer) pp. 63–150

[9] Taralli E, Portesi C, Lolli L, Monticone E, Rajteri M, Novikov I and Beyer J 2010 *Supercond. Sci. Technol.* **23** 105012

[10] Hattori K, Kobayashi R, Numata T, Inoue S and Fukuda D 2018 *J. Low Temp. Phys.* **193** 217

[11] Irwin K D, Hilton G C, Wollman D A and Martins J M 1998 *J. Appl. Phys.* **83** 3978

[12] Bennett D A, Swetz D S, Horansky R D, Schmidt D R and Ullom J N 2012 *J. Low Temp. Phys.* **167** 102

[13] Bennett D A, Swetz D S, Schmidt D R and Ullom J N 2013 *Phys. Rev. B* **87** 020508

[14] Morgan K M, Pappas C G, Bennett D A, Gard J D, Hays-Wehle J P, Hilton G C, Reintsema C D, Schmidt D R, Ullom J N and Swetz D S 2017 *Appl. Phys. Lett.* **110** 212602

[15] Wang Z, Zhang W, Miao W, Liu D, Zhong J Q and Shi S C 2018 *IEEE Trans. Appl. Supercond.* **28** 2100204

[16] Geng Y, Zhang W, Li P Z, Zhong J Q, Wang Z, Miao W, Ren Y, Wang J F, Yao Q J and Shi S C 2020 *J. Low Temp. Phys.* **199** 556

[17] Hattori K, Kobayashi R, Takasu S and Fukuda D 2020 *AIP Advances* **10** 035004

[18] Lolli L, Taralli E, Rajteri M, Numata T and Fukuda D 2013 *IEEE Trans. Appl. Supercond.* **23** 2100904

[19] Lindeman M A, Bandler S, Brekosky R P, Chervenak J A, Figueroa-Feliciano E, Finkbeiner F M, Li M J and Kilbourne C A 2004 *Rev. Sci. Instrum.* **75** 1283

[20] Kozorezov A G, Wigmore J K, Martin D, Verhoeve P and Peacock A 2006 *Appl. Phys. Lett.* **89** 223510

[21] Lolli L, Brida G, Degiovanni I P, Gramegna M, Monticone E, Piacentini F, Portesi C, Rajteri M, Ruo Berchera I, Taralli E and Traina P 2011 *Inter. J. Quant. Inform.* **9** 405

[22] Zhang W, Wang Z, Zhong J Q, Li P Z, Geng Y, Miao W, Ren Y, Zhou K M, Yao Q J and Shi S C 2021 *IEEE Trans. Appl. Supercond.* **31** 2101205